Geophysical Research Letters

RESEARCH LETTER
10.1029/2021GL097239

Wave, Vortex and Wave-Vortex Dipole (Instability Wave): Three Flavors of the Intra-Seasonal Variability of the North Equatorial Undercurrent

Chuanyu Liu[1,2,3], Ling Feng[1,3], Armin Köhl[4], Zhiyu Liu[5], and Fan Wang[1,2,3]

[1]CAS Key Laboratory of Ocean Circulation and Waves, Institute of Oceanology, Chinese Academy of Sciences (IOCAS), Qingdao, China, [2]Marine Dynamic Process and Climate Function Laboratory, Pilot National Laboratory for Marine Science and Technology (Qingdao) (QNLM), Qingdao, China, [3]Center for Ocean Mega Science, Chinese Academy of Sciences, Qingdao, China, [4]Institute of Oceanography (ifm), Center for Earth System Research and Sustainability (CEN), University of Hamburg, Hamburg, Germany, [5]State Key Laboratory of Marine Environmental Science, and Department of Physical Oceanography, College of Ocean and Earth Sciences, Xiamen University, Xiamen, China

Abstract Intra-seasonal variations have been frequently observed in the North Equatorial Undercurrent (NEUC) jets, yet their dynamical nature remains elusive. Based on field observations and model results, we identify three flavors of the ISVs: Wave (accounting for 10%), *wave-vortex dipole* (WVD) (20%) and vortex (70%). The wave flavor refers to a Rossby wave, the WVD flavor consists of a pair of counter-rotating vortices, and the vortex flavor refers to a sub-thermocline monopole eddy. To our knowledge, the WVD is identified for the first time and is found characterized by a unique dynamical feature: It manifests both as a second baroclinic mode-like Rossby wave and as a pair of dipole-like sub-thermocline eddies. It is further identified as a second baroclinic mode-like Rossby wave-initiated *instability wave* in an equilibrium being fueled by baroclinic conversion. These results indicate that mesoscale instability waves are an important component of subthermocline intra-seasonal and mesoscale variations.

Plain Language Summary At the depths of 200–1,000 m of the Pacific Ocean between 10°N and 18°N, the North Equatorial Undercurrent consisting of several jets flows eastward with mean velocity of ~5 cm s^{-1}. But it is not simply a steady current; instead, eastward and westward perturbations interlace, with an oscillation period of 70–120 days, which is called intra-seasonal variations (ISVs). These variations are known to exist from previous field observations, but their dynamical nature remains elusive. Here we present that they are possibly associated with three distinct flavors of subsurface mesoscale activities with a length scale of O(100 km). They are called, "vortex wave", "wave-vortex dipole" and "vortex". Among them, the wavevortex dipole flavor is an instability wave, dynamically intermediate between vortex wave and vortex, which might be an important component of oceanic intra-seasonal and mesoscale variations.

Key Points:

- Three flavors of the sub-thermocline variability—wave, vortex (mesoscale eddy) and wave-vortex dipole (WVD)—of the North Equatorial Undercurrent are identified
- The WVD consists of a pair of antisymmetric vortices and is characterized by lens-like temperature anomalies
- The WVD is identified as a second baroclinic mode-like Rossby wave-initiated instability wave fueled by baroclinic conversion

Supporting Information:

Supporting Information may be found in the online version of this article.

Correspondence to:

L. Feng and F. Wang,
lingfeng@qdio.ac.cn;
fwang@qdio.ac.cn

Citation:

Liu, C., Feng, L., Köhl, A., Liu, Z., & Wang, F. (2022). Wave, vortex and wave-vortex dipole (instability wave): Three flavors of the intra-seasonal variability of the North Equatorial Undercurrent. *Geophysical Research Letters*, *49*, e2021GL097239. https://doi.org/10.1029/2021GL097239

Received 30 NOV 2021
Accepted 19 MAY 2022

1. Introduction

In the tropical Pacific Ocean, the eastward flowing North Equatorial Undercurrent (NEUC; Wang et al., 2015) is a significant component of the sub-thermocline circulation system. Usually, the NEUC consists of three eastward jets, which are located at ~9°, 13° and 18°N, respectively, with a meridional scale of ~1.5° for each (Qiu, Rudnick, et al., 2013). Vertically, they are constrained between isopycnal layers of σ_θ = 26.8 and 27.6 kg m^{-3} (~200–1,000 m; Qiu, Chen, & Sasaki, 2013, Qiu, Rudnick, Chen, 2013). The NEUC jets transport intermediate water eastward with a mean velocity of 2–5 cm s^{-1} (L. Zhang et al., 2017; Qiu, Rudnick, et al., 2013; Wang et al., 2015; Yuan et al., 2014). As such, the NEUC jets play an important role in the transport of tropical waters.

In the past decade, a significant progress of the NEUC jets study is the discovery and characterization of its intra-seasonal variations (ISVs) based primarily on two subsurface moorings at 10.5°N and 13°N of 130°E (L. Zhang et al., 2017). In particular, it is found that the NEUC jets there share a similar feature: they oscillate with a period of 70–120 days, that is, the ISVs. The magnitude of ISVs reaches to 30 cm s^{-1}, much larger than its long term mean of ~5 cm s^{-1}. ISVs are strongest in sub-thermocline (~400–700 m) and become weaker upward (and possibly downward too). They are well distinguished from the ISVs of the westward North Equatorial Current (NEC) which are surface-intensified (L. Zhang et al., 2017). Therefore, it can be concluded that ISVs of the NEUC jets are a well-defined and significant sub-thermocline phenomenon of the tropical Pacific Ocean.

However, to date the dynamical nature of ISVs remains elusive, except for possible existence of second baroclinic mode Rossby waves by L. Zhang et al. (2017) based on the surface-intensified first empirical orthogonal function (EOF) mode. In addition, the ISVs may be caused by mesoscale eddies, as the eddies (generated by triad baroclinic Rossby waves) are argued to induce the mean NEUC jets (Qiu, Chen, & Sasaki, 2013); in fact, subsurface eddies are detected using eddy-resolving numerical models there (Xu et al., 2019). Yet, it is almost impossible to identify the processes solely based on the mooring observations, due to the lack of horizontal coverage. Therefore, this problem is investigated with outputs of an eddy-resolving numerical model in the present study. For the first time to our knowledge, we find an unanticipated component of the ISVs which show interesting features and important physical implications.

In Section 2, we introduce a new mooring, the model data, and all the methods applied. In Section 3, we present three prototypical flavors of the ISVs in the NEUC jets, with a special focus on the dynamics of the newly identified wave-vortex dipole. Finally, we give summary and discussions in Section 4.

2. Data and Methodology

2.1. Mooring Observation

The velocity data analyzed in this study were collected by a moored float deployed at 130°E, 12.5°N (one site of the Scientific Observing Network of the Chinese Academy of Sciences, CASSON; Wang et al., 2016) for the period of December 2016 to January 2018. This site is located at one core of NEUC jets (Qiu, Rudnick, et al., 2013). Two acoustic Doppler current profilers (ADCPs) (75-kHz) were equipped on a main float at ∼500 m depth, looking upward and downward, respectively, measuring the velocity of upper ∼1,000 m every 10 min.

2.2. Eddy-Resolving Model Outputs

To reveal the 3-D structure of the ISVs and their dynamics, daily outputs of temperature and velocity of the Mercator Ocean reanalysis product (version GLORYS12V1 and PSY4QV2R2, referred to as MO hereafter) for the period of years 1993–2019 (27 years) are employed. The MO model has a quasi-global domain from 80°S to 90°N with a resolution of 1/12°, and with 50 vertical levels with a resolution ranging from 1 m at the surface to 450 m near the bottom (Lellouche et al., 2013, 2018).

2.3. Composition of the ISVs

To obtain general structures of the ISVs, we composite 40 daily samples of each flavor obtained along their tracks. Since all the flavors travel almost along the zonal direction (without obvious meridional shift), the longitudes of each sample vary while the latitudes keep the same. (We note that the composite structures are statistically significant in that the standard deviations are nearly 2 orders small than the mean values; figures not shown).

2.4. Okubo-Weiss (OW) Parameter

To quantitatively discriminate the three flavors, the Okubo-Weiss (OW) parameter, formulated as $ow = (u_x - v_y)^2 + (u_y + v_x)^2 - (v_x - u_y)^2$, is adopted. ow is usually used for identifying mesoscale eddies with closed streamlines (Isern-Fontanet et al., 2003, 2006; Okubo, 1970; Weiss, 1991). For a curved flow with negative ow, the smaller the ow, the more likely it is marked as an eddy because its relative vorticity (the third term) overwhelms both the shear and normal strains (the first two terms).

2.5. Barotropic and Baroclinic Conversion Rate

To identify the driving force of the ISVs, we calculate the barotropic and baroclinic energy conversion rate (BTR and BCR) associated with them. Here, following von Storch et al. (2012) and Feng et al. (2022), $BTR = \overline{u'u'}\frac{\partial \overline{U}}{\partial x} + \overline{u'v'}\left(\frac{\partial \overline{U}}{\partial y} + \frac{\partial \overline{V}}{\partial x}\right) + \overline{v'v'}\frac{\partial \overline{V}}{\partial y}$ and $BCR = -\frac{g^2}{\rho_0^2 N^2}\left(\overline{u'\rho'}\frac{\partial \overline{\rho}}{\partial x} + \overline{v'\rho'}\frac{\partial \overline{\rho}}{\partial y}\right)$, where U, V and ρ are the monthly climatology of zonal and meridional velocities and density, respectively, obtained over 27 years (1993–2019); u', v' and ρ' are the daily anomalies relative to U, V and ρ, respectively; ρ_0 is a reference density and N^2 is the squared buoyancy frequency; the operator $\overline{(*)}$ denotes a composite.

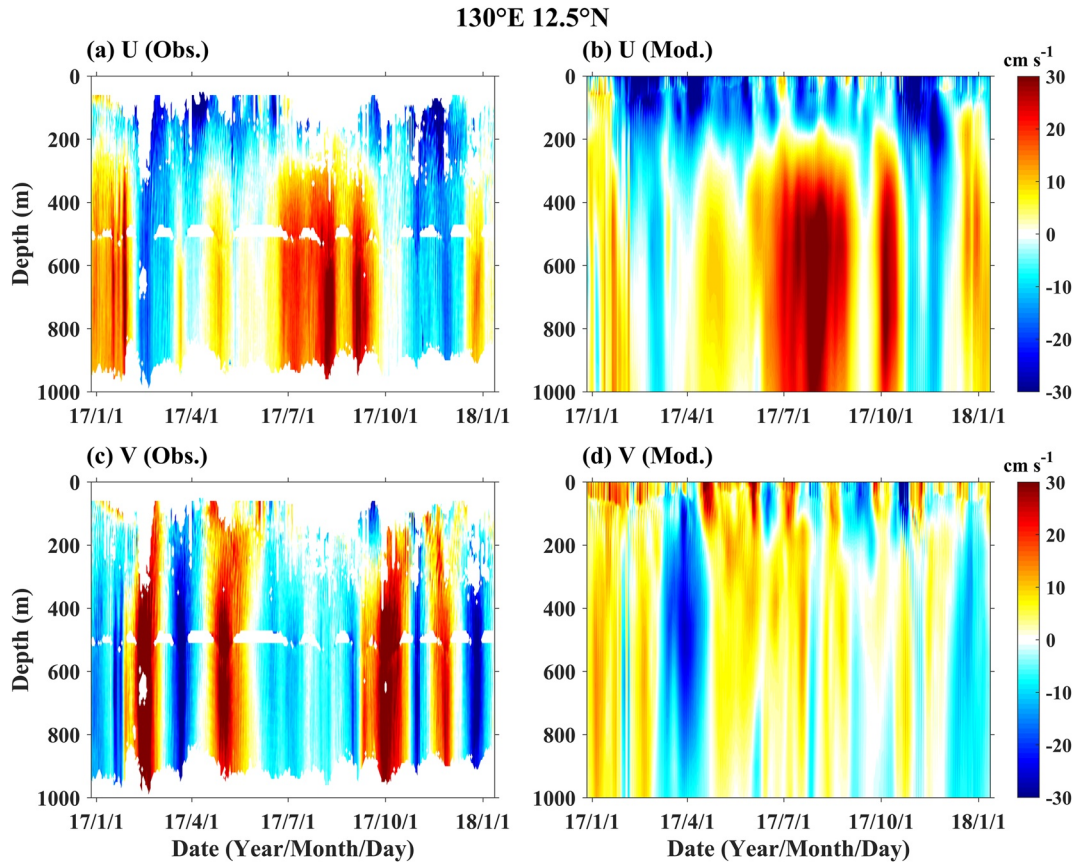

Figure 1. (a) Observed daily mean zonal and (c) meridional velocities. Blank area denotes data missing. (b and d), the same as (a and c) respectively but from model outputs.

3. Results

3.1. ISVs of NEUC in Observations and Model

The new moored velocity observations captured again the westward flowing NEC in the upper 300 m and the intermittent eastward flowing NEUC below; the magnitude of both reached 30 cm s^{-1} (Figure 1a). The ISVs of the NEUC jets were also clearly displayed. From case to case, their magnitude ranged from 5 to 30 cm s^{-1} for both the zonal and meridional velocities. Power spectral density (PSD) analysis showed a period of 70–120 days, the same as that identified at 130°E, 10.5°N and 13°N by L. Zhang et al. (2017).

Similar to the observations, the MO model velocities during the same period also show the NEC-NEUC structure vertically and magnitude-varying ISVs with similar period (Figures 1b and 1d). However, the modeled sub-thermocline velocities are smaller, particularly for the meridional velocities, which should be caused by the spatial variations of the ISVs in the model. Whereas, the multi-core NEUC jets are clearly reproduced by the model (Figure S1 in Supporting Information S1). Therefore, it can be concluded that the MO faithfully captures the main feature of NEUC and the ISVs, paving a way to investigating the characteristics and dynamics of the ISVs.

3.2. Three Flavors of the Sub-Thermocline ISVs

For convenience, the eddy kinetic energy (EKE) is taken as a proxy of the sub-thermocline ISVs, which is calculated with the velocity anomalies (u', v'; definition in Data and Method). By visual examination, we identify three primary flavors of the sub-thermocline ISV during the period of years 1993–2019 (Figure 2). Here, for the ease of comparison and presentation, we select a 1-year period (August 2014–July 2015) when the three flavors occurred successively, and show their propagation at two model depths, 380 and 1,062 m, representative for the

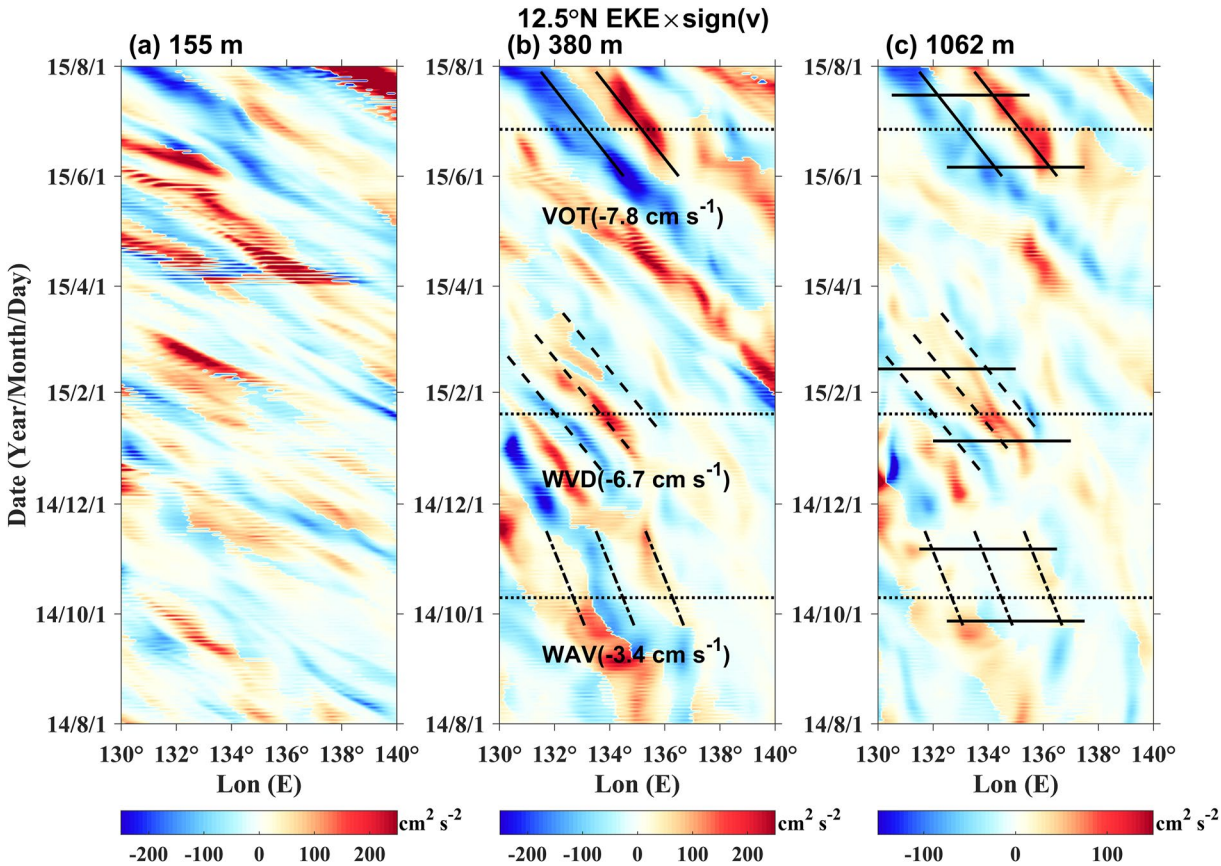

Figure 2. Time-longitude plot of eddy kinetic energy (EKEs) × sign (v) ($cm^2\ s^{-2}$) at (a) 155, (b) 380 and (c) 1,062 m. The detected three flavors of Intra-seasonal variations and corresponding isophases are marked (in b and c) and used for propagation speed calculation (insets in b). The horizontal dotted lines show the dates as shown in Figures 4a–4c. The horizontal thick lines in (c) show the temporal and zonal bands over which 40 daily samples are selected for the composites shown in Figures 3 and 4d–4k.

sub-thermocline; we also plot the EKE at 150 m for comparison. The three flavors are marked as WAV, WVD, and VOT, respectively (Figures 2b and 2c). Note that we use positive (negative) sign of EKE to represent variations with northward (southward) velocity component. Evidently, the EKE at 155 m was generally smaller than, and its propagation properties also differed from, that at 380 and 1,062 m, indicating that the sub-thermocline variations are indeed separated from the upper layer variations. In contrast, the EKE at those two depths shows much similarity in propagation properties, demonstrating that the sub-thermocline ISVs are vertically coherent through a 600–700 m thick layer, consistent with the observations.

The flavor WAV occurred during September–November 2014 with EKE of 100–200 $cm^2\ s^{-2}$. Horizontally, its EKE shows three strips featured as a "positive-negative-positive" structure, indicating presence of northward-southward-northward velocities; vertically, it is peaked at ~541 m in velocity and covers a depth range from ~200 to ~1,000 m. To obtain a prototypical structure of this flavor, we compose all the daily WAV signals (40 samples) along its track as shown in Figure 2c. The result (Figure 3a) shows that WAV is manifested as a Rossby wave according to its velocity pattern, which zonally spans ~4° with a wave crest and a wave trough; the wave-shaped meandering flow of WAV is particularly evident at the middle depths. A daily structure of the same flow pattern is shown in Figure 4a. Corresponding composite temperature anomalies are positive around the crest and negative around the trough (Figure 3a).

The flavor WVD occurred near the same region from December 2014 to March 2015 with EKE above 200 $cm^2\ s^{-2}$ (Figures 2b and 2c). Horizontally, it also has three EKE strips showing a "negative-positive-negative" structure; vertically, it is peaked at ~541 m and covers a similar depth to WAV (Figure 3b). Compared to WAV, WVD shows a similar structure in EKE, but with much larger magnitude. On the one hand, it resembles a Rossby wave; on the

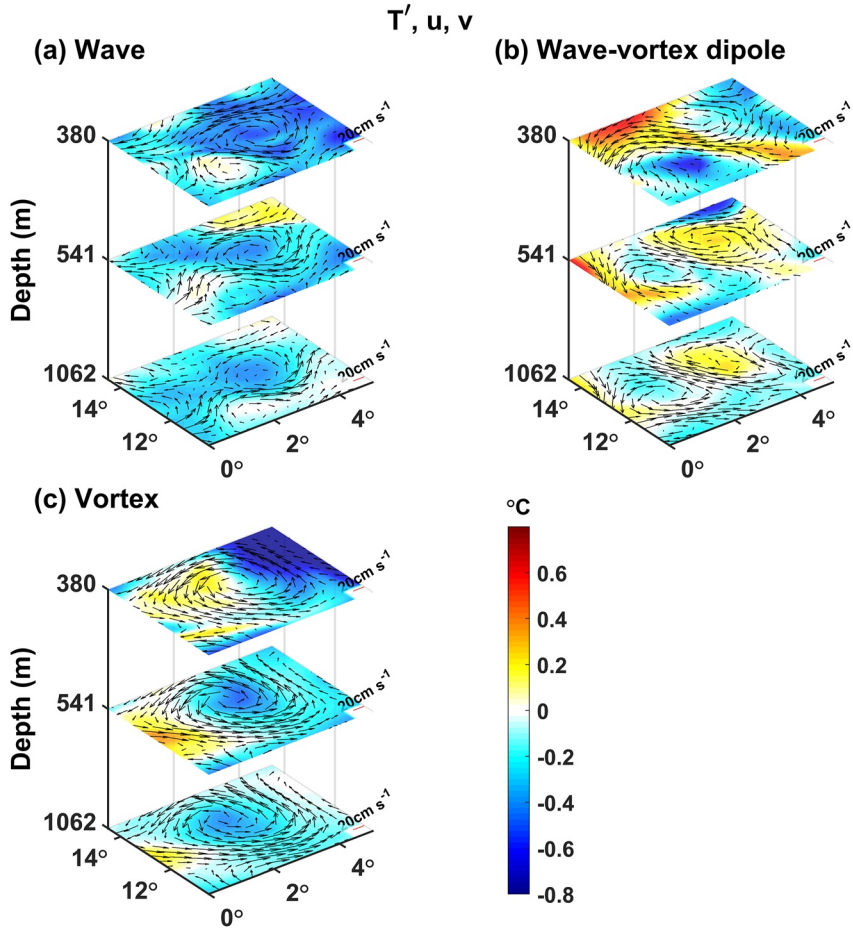

Figure 3. Composite temperature anomalies (shading) and total velocities (mean + anomaly; arrows) of the three flavors.

other hand, the associated flows rotate so fast that it is manifested as a pair of counter-rotating vortices (eddies). A daily WVD (Figure 4b) confirms this property. Quite surprisingly, the two vortices appeared and disappeared simultaneously, and moved westward jointly. As will be demonstrated below, physically it was not a normal wave, nor a random combination of two isolated eddies. Here, we term this structure as a *wave-vortex dipole* (WVD). The cyclonic and anti-cyclonic vortices of the WVD induce biconcave and biconvex lens-like temperature anomalies, respectively: The composite temperature anomalies within the cyclonic (anticyclonic) vortex was positive (negative) at 380 m and negative (positive) at 541 and 1,062 m (Figure 3b).

About three months later (June–August 2015), a third flavor VOT with the strongest EKE (200–300 $cm^2\ s^{-2}$) showed up. Different from WAV and WVD, it has only two EKE strips showing a "negative-positive" structure (Figures 2b and 2c). We thus recognize it as a typical subsurface cyclonic vortex (mesoscale eddy; Figures 3c and 4c). Vertically, the core of the eddy is also located at 541 m where the EKE and rotational speeds are maximum (Figure 3c). It is associated with biconvex lens-like temperature anomalies, similar to that of the subsurface cyclonic eddies in the Indian Ocean (Yang et al., 2019).

For generality, we summarize the characteristics of them as below. The streamlines of the major structure of the "WAV" are not well closed, but manifest as wave-like or meander-like structure and with at least one wave length; weak vortexes adjacent with the meanders might show up. In contrast, the streamlines of the major structure of the "WVD" and "VOT" are well closed (see Section 3.3), but "WVD" manifests as two prominent back-to-back vortexes, while "VOT" manifest as a strong monopole vortex. To illustrate them, we draw schematic structure (purple curves) in Figures 4a–4c, and also show more WAV and WVD examples in Figure S3 in Supporting Information S1. To what extent the streamlines of the major structure are closed is further quantitatively determined

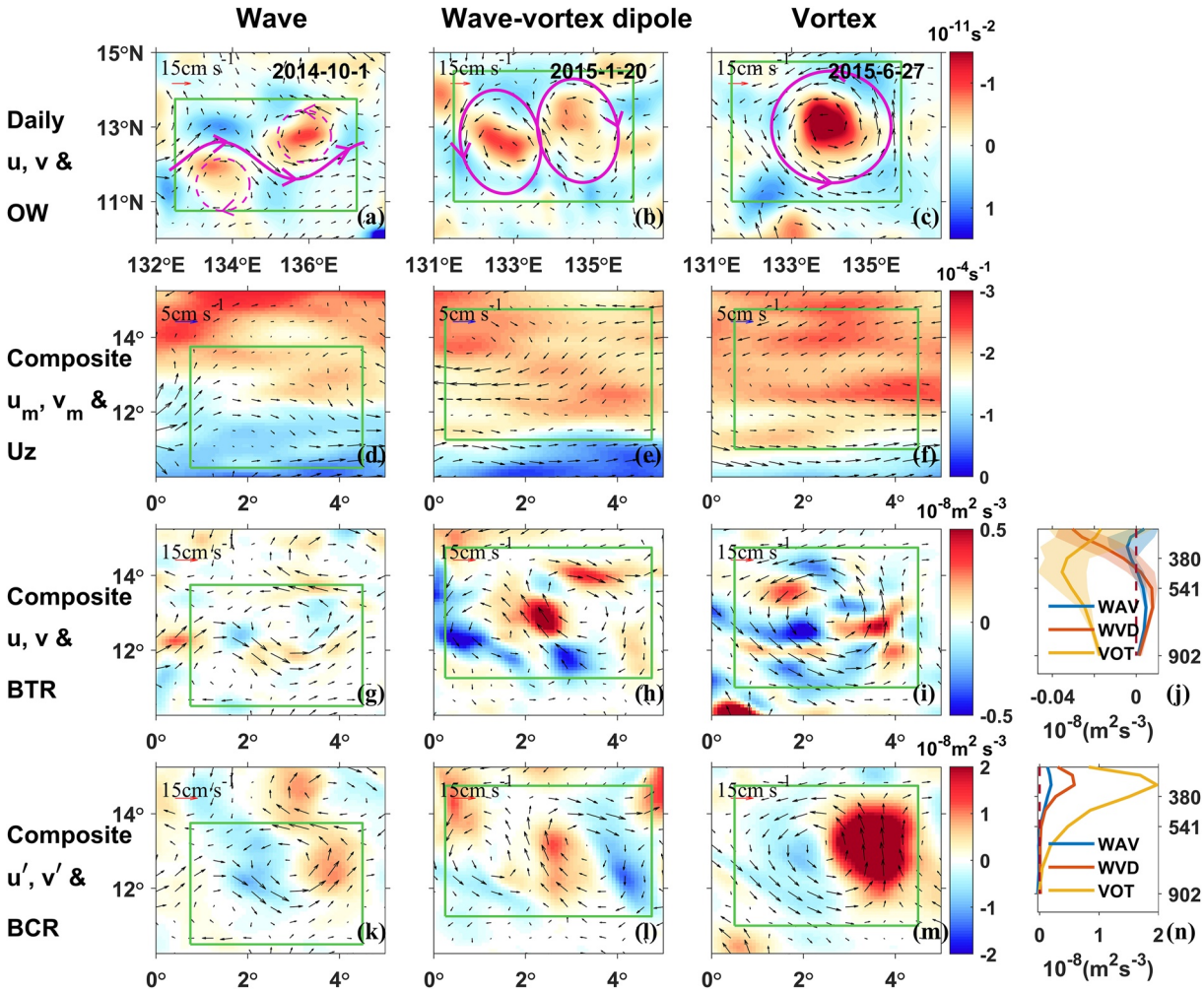

Figure 4. (a–c) Daily velocities (arrows) and Okubo-Weiss (OW) parameters (shading, after a 0.5° × 0.5° moving smooth) of the three flavors at 541 m, with the purple curves schematizing their major structures. (d–f) Composite monthly climatological velocities (arrows) and vertical shear (shading) of zonal velocity between 380 and 541 m. (g–i) Composite total (mean + anomaly) velocities (arrows) and barotropic (BTR) (shading). (k–m) Composite anomalous velocities (arrows) and baroclinic (BCR) (shading). (j and n) Flavor-associated area-mean overall BTR and BCR; the shading indicates the standard deviations (which are small and invisible in n); the areas for overall BTR and BCR calculation are shown as green boxes in (d–m), which cover the full area of each flavor.

using *ow*. After examination of these and other samples, we find that the magnitude of the negative *ow* for a WAV is usually $>-1\times10^{-11}$ s^{-2}, for a WVD flavor is $\leq-1\times10^{-11}$ s^{-2} and for a VOT flavor is $\leq-2\times10^{-11}$ s^{-2}. Those values are taken as the criteria for determination of the three flavors later on.

As such, the three kinds of flavors are frequently detected in the NEUC jets region in the model. By additionally apply some common criteria for all the three flavors, including the life span ≥21 days (the low bound of the ISV period), the horizontal characteristic scale criterion ≥2.5° (to ensure mesoscale), and the maximum EKE ≥ 100 cm^2 s^{-2} (to ensure significant signal/noise ratio), we find totally 40 sub-thermocline events during 1993–2019 and between 130° and 140°E along 12.5°N. Among them, eight events (account for 20%) were WVDs and 28 events (70%) were VOTs (eddies), both of which were associated with higher EKE (above 200 cm^2 s^{-2}); four WAVs (10%) with EKE ranging between 100 and 200 cm^2 s^{-2} were also detected. These results imply that the observed ISVs of NEUC may be due to the passing through of one or more of the three flavors. In the particular cases as observed at 130°E and 12.5°N during December 2016 to January 2018 (Figures 1a and 1c), the EKE was persistently above 300 cm^2 s^{-2}, indicating that the ISVs were most likely caused by mesoscale eddies or WVDs. However, the EKE of some other cases, for example, at 130°E, 10.5°N and 13°N during October 2014

to September 2015 (Figures 2a–2d of L. Zhang et al., 2017), was weaker and showed a large variance, indicating that the corresponding ISVs were probably included all three flavors.

3.3. Dynamical Properties of the WVD

Among the three sub-thermocline flavors, the WAV and VOT are well known mesoscale features. Looking insight into deeper layers, it is revealed the detected WAV, which has a velocity peak below the thermocline (~500 m; Figure 3a), actually is associated with another out-of-phase peak at ~2000 m (Figure S2 in Supporting Information S1); jointly, this flavor is most likely a second baroclinic mode Rossby wave because its characteristic vertical scale (covering 100–4,000 m) and structure (with two significant out-of-phase peaks) resemble a theoretical second baroclinic Rossby wave well (Pedlosky, 1987). However, considering the complexity in top and bottom conditions and the existence of the mean flow, which may modify the normal mode structure (LaCasce, 2017), we would only call this wave as a second baroclinic mode-*like* Rossby wave hereafter. Subsurface eddies were already detected in this latitude band in previous studies using either model outputs (Xu et al., 2019) or Argo profile data (Z. Zhang et al., 2017). By contrast, the WVD, to the best of our knowledge, is not yet depicted and interpreted in previous studies. Therefore, in this section, we focus on the dynamical properties of the WVD, along with a comparison with the other two flavors.

On the one hand, the velocity field suggests that each vortex of the WVD is a mesoscale eddy-like coherent feature, with strong vorticity and closed streamlines. Among the three flavors, *ow* of the Rossby wave is smallest (down to -1×10^{-11} s^{-2}, with the area-mean of 0.170×10^{-11} s^{-2}), while *ow* of the eddy is negative with the largest magnitude ($<-2 \times 10^{-11}$ s^{-2} and an area-mean of -0.035×10^{-11} s^{-2}); in comparison, *ow* of the two vortices of the WVD is negative with a moderate magnitude (-2×10^{-11} s^{-2} ~ -1×10^{-11} s^{-2} and an area-mean of 0.046×10^{-11} s^{-2}) (Figures 4a–4c). In addition to the strong vorticity and closed streamlines as eddies, the temperature anomalies associated with both vortices (Figure 3b) are also similar with the individual subsurface eddies observed by Argo floats (Z. Zhang et al., 2017) and Conductivity-Temperature-Depths (CTDs) (Yang et al., 2019). On the other hand, the WVD also shows features of a Rossby wave, though with differences. The cyclonic and anti-cyclonic vortices resemble an idealized Rossby wave, being manifested as two opposite phases in the zonal direction. They propagated westward jointly (Figures 4h and 4l).

The morphological and physical contrasts demonstrate that the WVD may be a process that is at a dynamical stage between linear Rossby waves and nonlinear eddies. The WVD kept its structure for more than 3 months, without developing into other forms till it quickly decayed, which means that it was in an equilibrium during most of the period. The other two flavors evolved similarly, with each being geostrophically balanced during most of their propagation period (the mean Rossby number ($U_m / f L$) is 0.035, 0.046 and 0.053 for WAV, WVD and VOT respectively, where U_m is the maximum rotational velocity, L is the wavelength or diameters of the flavors and f is Coriolis parameter).

In order to identify the driving force of them, we calculate the BTR and BCR associated with the three flavors (Figures 4g–4n). The overall (area-mean) BTR associated with the WVD is positive between ~400 and ~1,000 m, with a maximum of 1×10^{-10} m^2 s^{-3} between 550 and 600 m (Figure 4j), which is, however, nearly two orders smaller than the BCR; so as the other two flavors. The BCR associated with all the three flavors shows alternative signs over their different phases (Figures 4k–4m): The nearly equal magnitudes of positive and negative BCR associated with the northward and southward flowing parts of the WAV lead to a small overall (area-mean) BCR (~0.1×10^{-8} m^2 s^{-3} at ~350 m); however, stronger positive BCR associated with northward and weaker negative BCR associated with southward flowing parts of both the WVD and VOT lead to large positive overall BCR (~0.6×10^{-8} and 2×10^{-8} m^2 s^{-3} at ~350 m, respectively). The overall BCR for all the three flavors gradually decreases to zero below 1,000 m (Figure 4n). The standard deviation of the BCR is very small, indicating stable energy conversion along its propagation; by contrary, that of the BTR is rather large due to high spatial variations (Figures 4g–4j). These results demonstrate that the three flavors were energized by the mean flow via primarily the baroclinic conversion.

Due to this dynamical nature, the WVD likely can be identified as a sub-thermocline *instability wave* which was in an equilibrium between gaining energy via primarily baroclinic energy conversion and losing energy via other mechanisms (not studied here). A linear harmonic Rossby wave-like perturbation may grow due to energy conversion from the background flow, however, at what stage it reaches the equilibrium should depend on the strength of

instability of the background flow. A strongly unstable flow may drive the perturbation to grow to eddies, while weakly unstable flow can only maintain an equilibrium like the WAV or WVD. We found that the background mean flows of the WAV, WVD and VOT are respectively weakly eastward, strongly westward, and meridionally well sheared with westward (eastward) flow in the north (south); their corresponding vertical shear are weakest, moderate and strongest, respectively (Figures 4d–4f), confirming this hypothesis.

Furthermore, according to the common vertical scale and structure of the sub-thermocline ISVs in this region (Figure S2 in Supporting Information S1), the WVD likely is the second baroclinic mode-like Rossby wave-initiated instability wave. This can be indicated by Feng et al. (2021), Feng et al. (2022) and Hochet et al. (2015), who found that in this latitudinal band (8°–18°N) the fastest-growing baroclinic instability is subsurface-intensified and is generated by interaction of a pair of counter-propagating second baroclinic Rossby waves. Whereas, due to complicated top and bottom boundary conditions and mean flows, how well this baroclinic mode fits a normal second baroclinic mode needs further studies. (By the way, the background flow will also modify the speed of a normal second baroclinic mode Rossby wave, whose theoretical speed is ∼–10 cm s^{-1} at a wavelength similar to the three flavors, contrasting the propagation speeds of –3.4, –6.7 and –7.8 cm s^{-1} cm s^{-1} for the WAV, WVD and VOT, respectively; Figure 2).

3.4. Comparing the WVD With Other Dipole-Like Processes

Previously, a widely-studied mesoscale phenomenon that consists of a pair of cyclonic and anti-cyclonic eddies is the *modon*, which is referred to a steady mesoscale equilibrium solution on the β-plane (Flierl et al., 1983; Hughes & Miller, 2017; Stern, 1975). An evident feature of modon is that its two vortices are usually generated separately, which merge after they encounter, preserve the form as a dipole and propagate jointly with a faster speed than Rossby wave but without a preferred direction; in addition, the axis between the two vortices of a modon is usually perpendicular to its propagation direction. Another less dynamically restricted name for a pair of cyclonic and anti-cyclonic eddies is simply *dipole*. Ni et al. (2020) showed widespread surface dipoles (∼30–40% of the identified surface eddies). Dipoles consisting of a surface cyclonic eddy and a subsurface anticyclonic eddy were also observed in oceans (L'Hegaret et al., 2014; Pidcock et al., 2013). However, the WVD here differs from the aforementioned modons/dipoles in all the mentioned features, because the former is intrinsically a sub-thermocline instability Rossby wave consisting of two opposite phases.

4. Summary and Discussions

In the present work, we detected three flavors of sub-thermocline mesoscale processes that contribute to the ISVs of the NEUC jets, including WAV, WVD and VOT. Among them, the WVD shows specific dynamical features: on the one hand, its two vortices are as strong as eddies, on the other hand, they jointly propagate westward without being separated until they disappeared at the western boundary, showing a feature of Rossby wave. The WVD is identified as a second baroclinic mode-like Rossby wave-initiated instability wave which is in a state of equilibrium being fueled by the mean flow via baroclinic conversion. It means that the WVDs, like the VOTs, play an important role in the energy cascade particularly at the mesoscale stage. To our knowledge, such a sub-thermocline WVD is revealed for the first time. The WVD and other flavors as well may also induce mixing in the sub-thermocline layers and contribute to sub-thermocline transport, worthy of further exploring.

The WVD is an important component of the mesoscale and intra-seasonal variations. They may preferably occur in the conditions of moderate baroclinic instability, which can only support a wave-like perturbation to grow to a limited magnitude, rather than a mature eddy. It implies that a so-called "eddy" observed under that kind of conditions might only be the misidentification of one vortex of a WVD.

Data Availability Statement

The mooring data source (via NPOCE project and at https://doi.org/10.5281/zenodo.5482814) and the global ocean eddy-resolving reanalysis model data (https://doi.org/10.48670/moi-00021, available after registration) are greatly appreciated.

Acknowledgments
Thanks to the three anonymous reviewers for their constructive suggestions which helped improve this manuscript. This study is supported by the Strategic Priority Research Program of Chinese Academy of Sciences (CAS) (XDB42000000), the National Natural Science Foundation of China (41976012, 41730534).

References

Feng, L., Liu, C., Kohl, A., Stammer, D., & Wang, F. (2021). Four types of baroclinic instability waves in the global oceans and the implications for the vertical structure of mesoscale eddies. *Journal of Geophysical Research: Oceans*, *126*(3), e2020JC016966. https://doi.org/10.1029/2020jc016966

Feng, L., Liu, C., Köhl, A., & Wang, F. (2022). Seasonality of four types of baroclinic instability in the global oceans. *Journal of Geophysical Research: Oceans*, *127*, e2022JC018572. https://doi.org/10.1029/2022JC018572

Flierl, G. R., Stern, M. E., & Whitehead, A. J. (1983). The physical significance of modons: Laboratory experiments and general integral constraints. *Dynamics of Atmospheres and Oceans*, *7*(4), 233–263. https://doi.org/10.1016/0377-0265(83)90007-6

Hochet, A., Huck, T., & Verdière, A. C. d. (2015). Large-scale baroclinic instability of the mean oceanic circulation: A local approach. *Journal of Physical Oceanography*, *45*, 2738–2754. https://doi.org/10.1175/jpo-d-15-0084.1

Hughes, C. W., & Miller, P. I. (2017). Rapid water transport by long-lasting modon eddy pairs in the southern midlatitude oceans. *Geophysical Research Letters*, *44*(24). https://doi.org/10.1002/2017gl075198

Isern-Fontanet, J., García-Ladona, E., & Font, J. (2003). Identification of marine eddies from altimetric maps. *Journal of Atmosphere Oceanic Technology*, *20*(5), 20772–20778. https://doi.org/10.1175/1520-0426(2003)20<772:IOMEFA>2.0.CO;2

Isern-Fontanet, J., Garcia-Ladona, E., & Font, J. (2006). Vortices of the Mediterranean Sea: An altimetric perspective. *Journal of Physical Oceanography*, *36*(1), 87–103. https://doi.org/10.1175/jpo2826.1

LaCasce, J. H. (2017). The prevalence of oceanic surface modes. *Geophysical Research Letters*, *44*(11), 097105–097111. https://doi.org/10.1002/2017GL075430

Lellouche, J. M., Greiner, E., Galloudec, O. L., Garric, G., Regnier, C., Drevillon, M., et al. (2018). Recent updates to the Copernicus marine service global ocean monitoring and forecasting real-time 1/12° high-resolution system. *Ocean Science*, *14*(5), 1093–1126. https://doi.org/10.5194/os-14-1093-2018

Lellouche, J. M., Le Galloudec, O., Drévillon, M., Régnier, C., Greiner, E., Garric, G., et al. (2013). Evaluation of global monitoring and forecasting systems at Mercator Ocean. *Ocean Science*, *9*(1), 57–81. https://doi.org/10.5194/os-9-57-2013

L'Hegaret, P., Carton, X., Ambar, I., Menesguen, C., Hua, B. L., Cherubin, L., et al. (2014). Evidence of Mediterranean water dipole collision in the Gulf of Cadiz. *Journal of Geophysical Research: Oceans*, *119*(8), 5337–5359. https://doi.org/10.1002/2014JC009972

Ni, Q., Zhai, X., Wang, G., & Hughes, C. W. (2020). Widespread mesoscale dipoles in the global ocean. *Journal of Geophysical Research: Oceans*, *125*(10). https://doi.org/10.1029/2020JC016479

Okubo, A. (1970). Horizontal dispersion offloatable particles in vicinity of velocity singularities such as convergence. *Deep-Sea Research*, *17*(3), 445–454. https://doi.org/10.1016/0011-7471(70)90059-8

Pedlosky, J. (1987). *Geophysical fluid dynamics*, (2nd edn). Springer-Verlag. https://doi.org/10.1007/978-1-4612-4650-3

Pidcock, R., Martin, A., Allen, J., Painter, S. C., & Smeed, D. (2013). The spatial variability of vertical velocity in an Iceland basin eddy dipole. *Deep-Sea Research Part I*, *72*, 121–140. https://doi.org/10.1016/j.dsr.2012.10.008

Qiu, B., Chen, S., & Sasaki, H. (2013). Generation of the north equatorial undercurrent jets by triad baroclinic rossby wave interactions. *Journal of Physical Oceanography*, *43*(12), 2682–2698. https://doi.org/10.1175/JPO-D-13-099.1

Qiu, B., Rudnick, D. L., Chen, S., & Kashino, Y. (2013). Quasi-stationary North Equatorial Undercurrent jets across the tropical North Pacific ocean. *Geophysical Research Letters*, *40*(3), 2183–2187. https://doi.org/10.1002/grl.50394

Stern, M. E. (1975). Minimal properties of planetary eddies. *Journal of Marine Research*, *40*, 57–74.

von Storch, J.-S., Eden, C., Fast, I., Haak, H., Hernández-Deckers, D., Maier-Reimer, E., et al. (2012). An estimate of the Lorenz energy cycle for the World Ocean based on the STORM/NCEP simulation. *Journal of Physical Oceanography*, *42*(12), 2185–2205. https://doi.org/10.1175/JPO-D-12-079.1

Wang, F., Song, L., Li, Y., Liu, C., Wang, J., Lin, P., et al. (2016). Semiannually alternating exchange of intermediate waters east of the Philippines. *Geophysical Research Letters*, *43*(13), 7059–7065. https://doi.org/10.1002/2016GL069323

Wang, F., Zang, N., Li, Y., & Hu, D. (2015). On the subsurface countercurrents in the Philippine Sea. *Journal of Geophysical Research: Oceans*, *120*(1), 131–144. https://doi.org/10.1002/2013JC009690

Weiss, J. (1991). The dynamics of enstrophy transfer in 2-dimensional hydrodynamics. *Physical Dynamics*, *48*(2–3), 273–294. https://doi.org/10.1016/0167-2789(91)90088-q

Xu, A., Yu, F., & Nan, F. (2019). Study of subsurface eddy properties in northwestern Pacific Ocean based on an eddy-resolving OGCM. *Ocean Dynamics*, *69*(4), 463–474. https://doi.org/10.1007/s10236-019-01255-5

Yang, G.-B., Zheng, Q., Xiong, X.-J., Yuan, Y., Zhuang, Z., Hui, Z., et al. (2019). Subsurface cyclonic eddies observed in the southeastern tropical Indian Ocean. *Journal of Geophysical Research: Oceans*, *124*(10), 7247–7260. https://doi.org/10.1029/2019JC015381

Yuan, D., Zhang, Z., Chu, P. C., & Dewar, W. K. (2014). Geostrophic circulation in the tropical North Pacific Ocean based on Argo profiles. *Journal of Physical Oceanography*, *44*(2), 558–575. https://doi.org/10.1175/JPO-D-12-0230.1

Zhang, L., Wang, F. J., Wang, Q., Hu, S., Wang, F., & Hu, D. (2017). Structure and variability of the north equatorial current/Undercurrent from mooring measurements at 130°E in the western Pacific. *Scientific Reports*, *7*(3), 1–9. https://doi.org/10.1038/srep46310

Zhang, Z., Zhang, Y., & Wang, W. (2017). Three-compartment structure of subsurface-intensified mesoscale eddies in the ocean. *Journal of Geophysical Research: Oceans*, *122*(3), 1653–1664. https://doi.org/10.1002/s2016JC012376